The Beta Drift of Baroclinic Vortices. Part I: Adiabatic Vortices

YUQING WANG*

Centre for Dynamical Meteorology and Oceanography, Monash University, Clayton, Victoria, Australia

GREG J. HOLLAND

Bureau of Meteorology Research Centre, Melbourne, Victoria, Australia

(Manuscript received 12 October 1994, in final form 8 August 1995)

ABSTRACT

The dynamics of the movement of an initially axisymmetric baroclinic vortex embedded in an environment at rest on a beta plane is investigated with a three-dimensional primitive equation model. The study focuses on the motion and evolution of an adiabatic vortex and especially the manner in which vertical coupling of a tilted vortex influences its motion. The authors find that the vortex movement is determined by both the asymmetric flow over the vortex core associated with beta gyres and the flow associated with vertical projection of the tilted potential vorticity anomaly. The effects of vortex tilt can be large and complex. The secondary divergent circulation is found to be associated with the development of potential temperature anomalies required to maintain a balanced state. The processes involved strongly depend on the vertical structure, size, and intensity of the vortex together with external parameters such as the earth rotation and static stability of the environment. As a result, simple relationships between vortex motion and the vertical mean relative angular momentum are not always applicable.

1. Introduction

It is well known that beta drift is a basic component of tropical cyclone motion. Since this motion arises from the interaction between the vortex circulation and the planetary vorticity gradient, its study is of importance to vortex dynamics in general.

The barotropic dynamics of the beta gyres and beta drift of tropical cyclone-scale vortices have been extensively investigated over the past few years (Elsberry and Abbey 1991). An initially symmetric vortex in an earth vorticity gradient will develop a pair of counter-rotating gyres (beta gyres) due to Rossby wave dispersion and multiscale interaction (Holland 1983; Chan and Williams 1987; Shapiro and Ooyama 1990; Smith et al. 1990). These asymmetric gyres have horizontal scales on the order of 1000 km and contribute to a relative flow across the vortex core that causes it to propagate poleward and westward (Fiorino and Elsberry 1989a; Carr 1989; Peng and Williams 1990; Smith and Ulrich 1990; Sutyrin and Flierl 1994). The outer vortex structure is instrumental in determining the amplitude and orientation of the asymmetric gyres, but there is very little sensitivity to the core region structure or intensity (Holland 1983; DeMaria 1985; Fiorino and Elsberry 1989b; Carr and Williams 1989).

Energetically, the beta gyres develop by extracting kinetic energy from the symmetric circulation of the vortex (Li and Wang 1994). This energy conversion is associated with momentum advection and meridional advection of planetary vorticity, with the latter being a principal process for the generation of the asymmetric circulation. The rate of asymmetric kinetic energy generation and gyre development increases with increasing relative angular momentum of the symmetric circulation. Li and Wang also found that, depending on the initial vortex structure, vortices may follow a variety of tracks ranging from a quasi-steady displacement to an erratic or a cycloidal track. This is due to the evolution of the beta gyres, which is characterized by development/decay, gyration, and radial movement.

Simple three-dimensional models with idealized conditions have recently been applied to the study of tropical cyclone motion. One purpose is to compare the motion response of the different layers when the cyclone has vertical structure. Considering the structure-dependent role of the beta effect in the barotropic models, circulations at different layers of a baroclinic cyclone might be expected to propagate with different velocities. However, Wang and Li (1992) used a 10-level primitive equation model on a beta plane, with no

* Current affiliation: Bureau of Meteorology Research Centre, Melbourne, Victoria, Australia.

Corresponding author address: Dr. Yuqing Wang, BMRC, GPO Box 1289K, Melbourne, Vic 3001, Australia.
E-mail: wzy@tracy.ho.bom.gov.au

heating or friction to show that the vortex remains vertically coupled by developing a secondary circulation. A vortex that was initially cyclonic at all levels drifted poleward and westward with a nearly height-independent speed, in a close analogy to the barotropic case. They suggested that the vertical structure affected the beta drift by changing the vertical mean relative angular momentum (MRAM) in a similar manner to that described by Shapiro and Ooyama (1990) for the horizontal structure. When the vortex turned anticyclonic with height, the vertical coupling was lost, and the upper anticyclonic part moved equatorward and westward, while the lower cyclonic part drifted poleward and westward. Thus, vertical coupling in a dry model cannot hold the upper anticyclone above the surface cyclone against the differential propagation arising from the beta effect.

Shapiro (1992) included simple representations of boundary drag, convective heating, and momentum transports in a three-layer model in which a tropical cyclone vortex was first spun up on an f plane for 48 h, then integrated on a beta plane. Differential advection of potential vorticity resulted in an asymmetric circulation in the middle layer that was very similar to that found in barotropic models, with a cyclonic (anticyclonic) gyre to the west (east). The flow between this gyre pair was not as uniform as in the barotropic models, but it clearly advected the vortex poleward and westward. Although the upper-layer anticyclone developed a pair of gyres of the opposite sense to those in the middle layer, their amplitude and impact was small compared to the middle-layer gyres.

Wang et al. (1993) and Holland and Wang (1995) observed considerable vertical tilt of a baroclinic vortex in vertically sheared environmental flow or on a beta plane with the environment at rest. They found that an adiabatic vertical circulation developed in such a way that the ascending (descending) motion occurred on the downtilt (uptilt) side of the vortex center. This vertical circulation was required to maintain the stable vertical tilt of the baroclinic vortex.

However, questions still remain about several aspects of the baroclinic dynamics of the beta drift. For example, the detailed vertical coupling mechanism and its relationship to vortex motion are still unknown. The aim of this paper is to examine the fundamental baroclinic dynamics of the beta drift of a three-dimensional adiabatic vortex by a comprehensive investigation of the vertical coupling mechanism and the effect of vertical structure. Section 2 briefly describes the numerical model and the vortex structure used in this study. The motion and evolution of a standard vortex are investigated in section 3. The influence of the vertical structure of the initial vortex and the sensitivity of the vortex motion to various parameters are evaluated in sections 4 and 5, respectively. Section 6 compares the motion of baroclinic vortex with that of an equivalent barotropic one. The last section contains the major findings and conclusions.

2. Numerical details

a. The baroclinic model

The baroclinic model used in this study is a dry three-dimensional primitive equation model on a beta plane, centered at 20°N. Using the vertical coordinate $\sigma = (p - p_t)/(p_s - p_t)$, the governing equations can be written as

$$\frac{\partial u}{\partial t} + u\frac{\partial u}{\partial x} + v\frac{\partial u}{\partial y} + \dot{\sigma}\frac{\partial u}{\partial \sigma} = fu - \frac{\partial \phi}{\partial x} - c_p\theta\frac{\partial P}{\partial x} + D_u, \quad (1)$$

$$\frac{\partial v}{\partial t} + u\frac{\partial v}{\partial x} + v\frac{\partial v}{\partial y} + \dot{\sigma}\frac{\partial v}{\partial \sigma} = -fu - \frac{\partial \phi}{\partial y} - c_p\theta\frac{\partial P}{\partial y} + D_v, \quad (2)$$

$$\frac{\partial \ln\pi}{\partial t} + u\frac{\partial \ln\pi}{\partial x} + v\frac{\partial \ln\pi}{\partial y} = -\left(\frac{\partial u}{\partial x} + \frac{\partial v}{\partial y}\right) - \frac{\partial \dot{\sigma}}{\partial \sigma}, \quad (3)$$

$$\frac{\partial \theta}{\partial t} + u\frac{\partial \theta}{\partial x} + v\frac{\partial \theta}{\partial y} + \dot{\sigma}\frac{\partial \theta}{\partial \sigma} = \frac{\dot{Q}}{c_p P} + D_\theta, \quad (4)$$

$$\frac{\partial \phi}{\partial P} = -c_p\theta, \quad (5)$$

where $P = (p/1000)^{R/C_p}$, $\pi = p_s - p_t$, and ϕ is the geopotential of σ surfaces. All other variables have their usual meanings. The pressure at the top of the model is $p_t = 100$ hPa. The model consists of M layers in the vertical from $\sigma = 0$ to 1, with the interfaces $\sigma_k = k/M$, $k = 1, 2, \cdots, M - 1$. All vertically dependent variables, u, v, θ, ϕ, are calculated on the middle of each layer, but the vertical velocity $\dot{\sigma}$ is staggered. For upper and lower boundary conditions, we require that fluid particles do not cross the $\sigma = 0$ and $\sigma = 1$ surfaces; that is,

$$\dot{\sigma} = 0, \quad \text{at} \quad \sigma = 0 \quad \text{and} \quad \sigma = 1. \quad (6)$$

In most of the numerical experiments presented in this study, we chose $M = 5$ to ensure that we had sufficient levels to be able to differentiate the vertical structure of the vortex circulation while maintaining a relatively simple configuration. The horizontal mesh of the model consists of 141 × 141 grid points with a uniform spacing of 25 km. All variables are defined at the same grid point on the σ surfaces. Sponge layers are applied to the north and south boundaries, as used

by Wang and Li (1992), and in the east–west direction all variables are cyclic. The governing equations are solved using a two-time-level explicit split scheme similar to that used by Gadd (1978). The procedure consists of an advection step with time step Δt_A followed by N adjustment steps with time step $\Delta t_L = \Delta t_A/N$.

For the advection stage, the governing equations become

$$\frac{\partial A}{\partial t} = -u\frac{\partial A}{\partial x} - v\frac{\partial A}{\partial y}, \tag{7}$$

where A denotes u, v, θ, or $\ln\pi$. Integration of this stage uses a fourth-order Lax–Wendroff scheme with splitting in the x and y directions. An important feature of the scheme is that, following McGregor (1986) and Leslie and Purser (1991), the advective change in the surface pressure field, $\ln\pi$, is saved at each model level; that is,

$$A\Pi = -u\frac{\partial \ln\pi}{\partial x} - v\frac{\partial \ln\pi}{\partial y} \tag{8}$$

is calculated from the fourth-order Lax–Wendroff scheme and stored. The value for π itself is not updated until during the geostrophic adjustment stage.

Defining the horizontal divergence by $D = (\partial u/\partial x + \partial v/\partial y)$, the governing equations for the adjustment stage become

$$\frac{\partial u}{\partial t} = fv - \frac{\partial \phi}{\partial x} - c_p\theta\frac{\partial P}{\partial x} - \dot\sigma\frac{\partial u}{\partial \sigma} + D_u, \tag{9}$$

$$\frac{\partial v}{\partial t} = -fu - \frac{\partial \phi}{\partial y} - c_p\theta\frac{\partial P}{\partial y} - \dot\sigma\frac{\partial v}{\partial \sigma} + D_v, \tag{10}$$

$$\frac{\partial \theta}{\partial t} = -\dot\sigma\frac{\partial \theta}{\partial \sigma} + \frac{\dot Q}{c_p P} + D_\theta, \tag{11}$$

$$\frac{\partial \ln\pi}{\partial t} = \int_0^1 (A\Pi - D)d\sigma, \tag{12}$$

$$\dot\sigma = (1-\sigma)\frac{\partial \ln\pi}{\partial t} + \int_1^\sigma (A\Pi - D)d\sigma, \tag{13}$$

$$\phi = \phi_s - \int_1^\sigma c_p\theta dP, \tag{14}$$

where ϕ_s is the surface geopotential, which is set to 0 in this study.

The forward–backward scheme (Mesinger 1977; Gadd 1978) is used for the time integration of the above adjustment stage. As suggested by Gadd (1980), the Coriolis terms are treated implicitly. For the horizontal differencing, we use a centered finite-difference scheme with second-order precision. The vertical differencing scheme is identical to that used by Arakawa and Lamb (1977). The horizontal diffusion terms D_u, D_v, and D_θ are incorporated into the model by a low-pass filtering operation similar to that used by Purser and Leslie (1988).

For the horizontal resolution chosen in this study, an adjustment time step $\Delta t_L = 60$ s was used, and the number of adjustment steps per advection step was chosen to be $N = 3$. These choices of the numerical model, including the vertical resolution, are all based on our sensitivity experiments with the model applied to the baroclinic vortices described in section 2a. We found that doubling the vertical resolution resulted in less than a 75-km change in vortex positions after a 5-day time integration. This resulted mainly from changes in vertical mean relative angular momentum (section 2c) arising from the nonlinear function of tengential wind with σ. We specifically address such changes in this paper for which the five-level resolution is quite acceptable.

b. *The shallow-water model*

For the comparison between the baroclinic and the equivalent barotropic vortex motion, we reduced the baroclinic model to a shallow-water equation model with a mean depth of 1 km and initialized with the vertical mean wind of the initial baroclinic vortex. The corresponding geopotential perturbation is obtained by solving the nonlinear balance equation similar to that discussed in Wang (1995) so that the barotropic vortices satisfy the gradient wind balance.

c. *Vortex structure*

The tangential wind profile of the baroclinic vortex used as the standard in the following runs (referred to as V_A) is defined as

$$V_T(r,\sigma) = V_m\left(\frac{r}{r_m}\right)\exp\left[1-\left(\frac{r}{r_m}\right)\right] \times \sin\left[\frac{\pi}{2}\frac{(\sigma+0.2)}{1.2}\right], \tag{15}$$

where r denotes radial distance from the vortex center, V_m the maximum tangential wind at the surface, and r_m the radius of maximum wind.

To consider the influence of the upper anticyclonic circulation on the motion of the vortex, we introduce the following anticyclone to the upper levels:

$$V_{TA}(r,\sigma) = \begin{cases} -V_0\left(\frac{r}{r_a}\right)\exp\left\{\frac{1}{2}\left[1-\left(\frac{r}{r_a}\right)^2\right]\right\} \\ \quad \times \sin\left(\pi\frac{r}{r_e}\right)E(\sigma), & r < r_e, \\ 0, & r \geq r_e \end{cases} \tag{16}$$

TABLE 1. The vortex parameters used in this study.

	V_0 (m s^{-1})	σ_c	r_a (km)	r_e (km)
V_A	0.0	—	—	—
V_B	5.0	0.7	260.0	1000.0
V_C	15.0	0.5	260.0	1000.0
V_D	15.0	0.7	260.0	1000.0

where

$$E(\sigma) = \begin{cases} \cos^2\left(\frac{\pi}{2}\frac{\sigma}{\sigma_c}\right), & \sigma \leq \sigma_c, \\ 0, & \sigma > \sigma_c. \end{cases} \quad (17)$$

We vary the anticyclone using the values of V_0, r_a, r_e, and σ_c given in Table 1; $V_m = 32$ m s^{-1}, and $r_m = 100$ km unless otherwise specified. The tangential wind profiles for the four vortices used in this study are given in Fig. 1. The standard vortex V_A is cyclonic through the depth of the model atmosphere. The other three vortices (V_B, V_C, and V_D) have the same structure as V_A in the lower levels but are different in the middle and upper levels. In the lower levels, V_B is similar to V_A, except that the cyclonic circulation at the mid-upper levels is somewhat weaker. Vortex V_D has a deeper upper anticyclonic circulation than V_c and is much more anticyclonic than V_B. These vortex structures are representative of real tropical cyclones (Frank 1977).

Following Wang and Li (1992), we define the MRAM of the vortex circulation as

$$\text{MRAM} = \frac{\int_0^1 \int_A v(r) r dA d\sigma}{\int_0^1 \int_A dA d\sigma}, \quad (18)$$

where A is the horizontal area within a radius R from the vortex center. Figure 2 shows the MRAM corresponding to the four vortices in Fig. 1 as a function of R. It can be seen that the total MRAM within the vortex circulation (about 1000 km from the vortex center) is largest in V_A and smallest in V_D.

The environment has a constant surface pressure of 1008.7 hPa and a thermal structure defined by the mean tropical atmosphere of Stevens et al. (1977):

$$\theta = 300 + \frac{\Gamma}{\kappa}\left[\left(\frac{1000}{p}\right)^{\kappa} - 1\right], \quad (19)$$

where $\kappa = R/c_p$, Γ is the mean static stability parameter, and we set $R\Gamma/g = 620$ m for our standard runs.

The numerical model is initialized with the axisymmetric vortices defined above, on an f plane centered at 20°N. The corresponding surface pressure and the thermal fields are in gradient wind balance and are obtained by solving the inverse balance equation in σ coordinates (Wang 1995). All four vortices have a warm-core structure, with a maximum potential temperature anomaly at about the middle level of the model. The vortex center at each level during the model integration is determined by the position of maximum potential

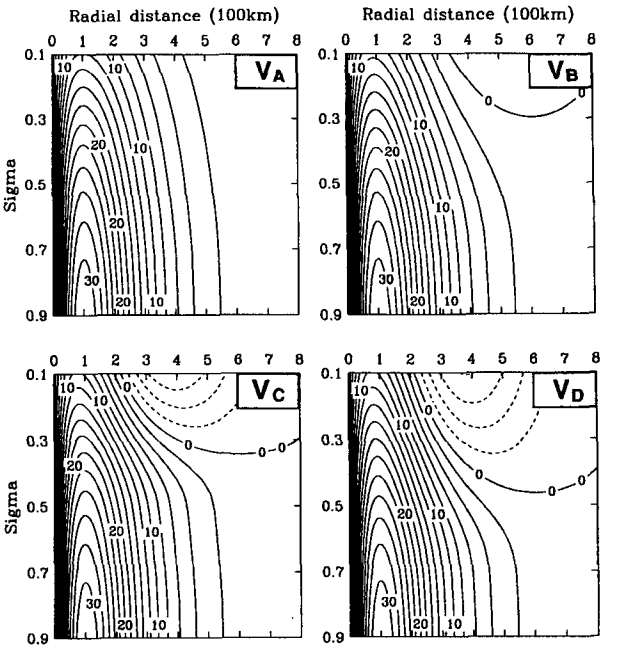

FIG. 1. Azimuthal wind profiles for the four vortices used in this study. Contour interval is 2 m s^{-1}.

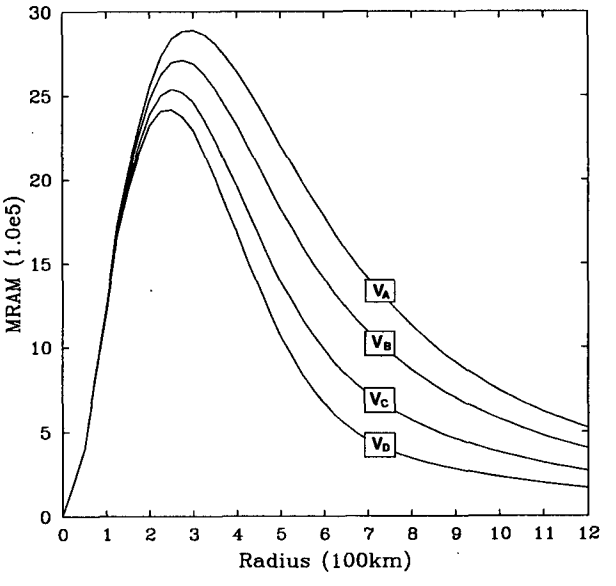

FIG. 2. The vertical mean relative angular momentum (MRAM) of the four vortices in Fig. 1 as a function of R. Unit is meters squared per second.

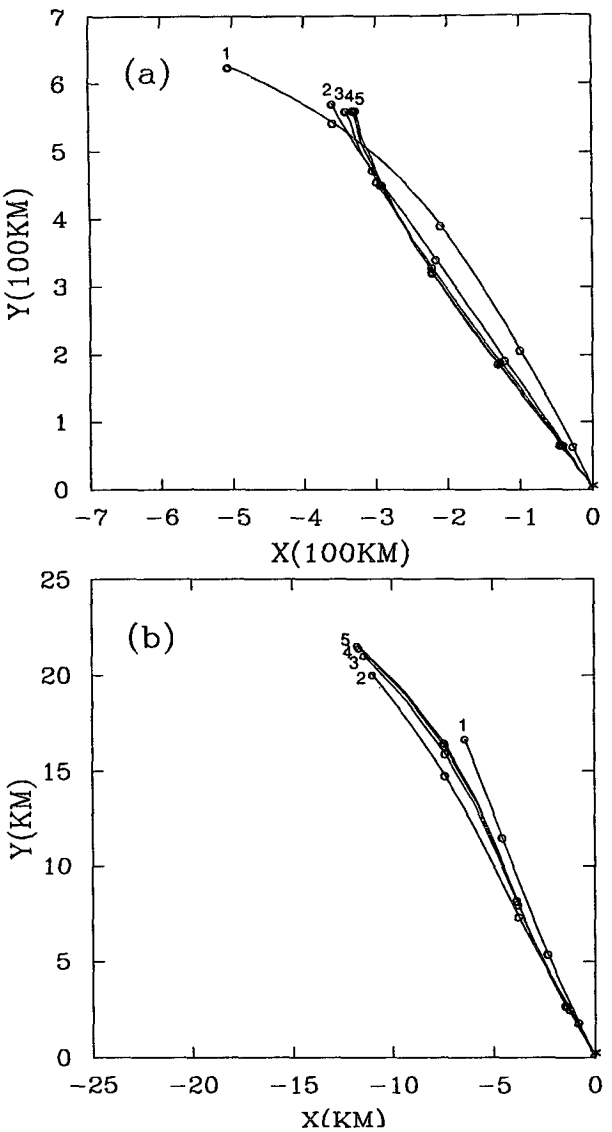

FIG. 3. Tracks of the standard vortex at all model levels (indicted by the level numbers; 5 is the lowest level): (a) 120 h (24-h positions shown) and (b) the initial 12 h (3-h positions shown).

vorticity (PV) objectively calculated by the method of Wang and Zhu (1989). The tracks of the vortices are defined by the maximum PV at the lowest model level ($\sigma = 0.9$).

We note that the necessary conditions for both inertial and barotropic instabilities are satisfied in V_C and V_D, but this does not seem to have affected our results. Flatau and Stevens (1989) found that the inertially unstable modes in the hurricane outflow layer have very small vertical scale and are likely stabilized by turbulence; thus, the coarse vertical resolution of the numerical model used in this study prevents immediate release of the inertial instability. Flatau and Stevens (1989) also found that barotropically unstable internal modes with an equivalent depth of 30 m and azimuthal wavenumber 1 would have an e-folding time of about 7 days. The 5-day time integration of this study is too short for the unstable modes to grow to substantial amplitude and affect the vortex motion. Further, linear analysis is applicable only to the early stages of growth when perturbation is very weak; nonlinearity may stabilize the unstable modes by wave–wave and wave–mean vortex interactions (Willoughby 1992, 1994).

Flatau and Stevens (1993) have indicated that outflow-layer instability may contribute to slow (periods of a few days) trochoidal motion of a tropical cyclone. But development of this instability depends on the horizontal structure and frequency of the environmental forcing. Since we have not included any environmental forcing other than the beta effect, barotropic instability is not expected to influence the vortex motion significantly. We also note that the influence of barotropic instabilities on vortex motion is negligible in the adiabatic experiments of Flatau and Stevens (1993). Thus,

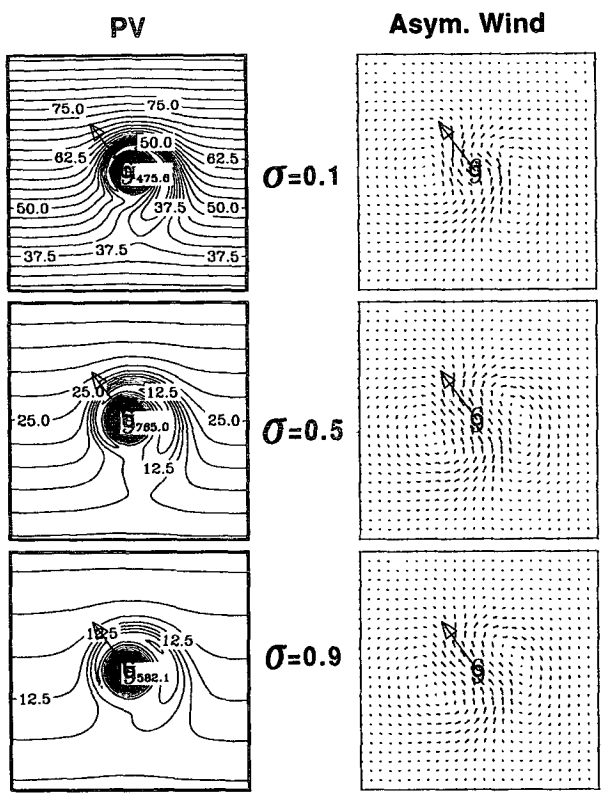

FIG. 4. Potential vorticity fields (left) and asymmetric wind vectors (right) at indicated levels for the standard vortex at 36 h. Contour interval in left panels is 2.5 × 10^{-8} K kg^{-1} m^2 s^{-1}. The maximum vectors in right panels are 1.83 in the top, 2.65 in the middle, and 2.85 m s^{-1} in the bottom. The domain shown in each panel is 2500 km × 2500 km; the cyclone symbol and arrow indicate the position and direction of motion of the vortex center at the lowest level.

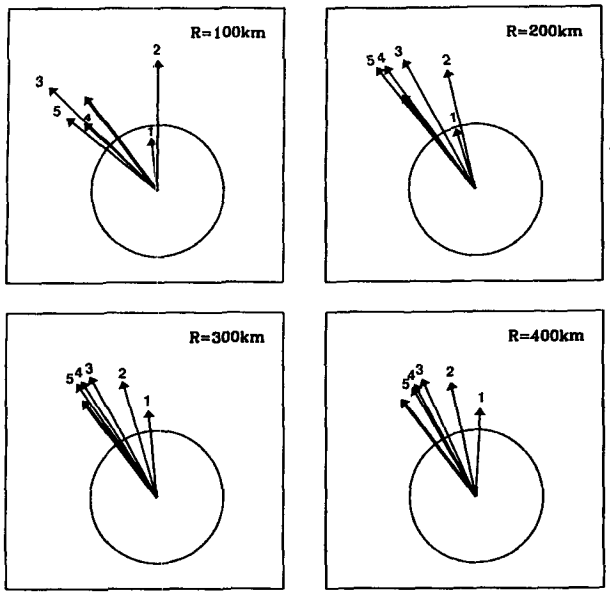

FIG. 5. Area mean asymmetric flow over the standard vortex center at different levels (indicated at the end of the arrows) after 48 h of integration. The circle indicates a speed of 1.0 m s^{-1}. The radius (R) used to calculate the mean flow is indicated in each frame; the thick arrow indicates the motion of the surface vortex.

the dynamical instability of the vortex to linear perturbations is not investigated in this study.

3. The motion and evolution of the standard vortex

a. Mean vortex motion

The standard vortex V_A moves poleward and westward (Fig. 3a). After 120 h of integration, V_A moved 328 km to the west and 561 km to the north, with an average speed of 1.64 m s^{-1} and direction of 330° from 24 to 120 h. This is comparable with that found in previous studies of barotropic and baroclinic vortices (e.g., Chan and Williams 1987; Wang and Li 1992). However, the track of the vortex has a slight cyclonic curvature during the first 12 h of integration and then an anticyclonic curvature, which arises from interactions between the circulations at different levels after the vortex tilts, as discussed in section 3b.

The PV fields after 36 h of integration (left panels in Fig. 4) have all the classic characteristics of a vortex moving on a beta plane, with anticyclonic PV anomalies to the east and cyclonic PV anomalies to the west. Associated with these PV anomalies is a pair of counterrotating beta gyres, forming an asymmetric flow over the vortex core that advects the vortex to the northwest (right panels in Fig. 4). The increasing northward gradient of PV with height is mainly related to the increase in the vertical gradient of the background potential temperature, and thus the decrease of vortex circulation dominates to produce a decreasing asymmetric flow (Fig. 5). This causes the vortex to tilt equatorward early in the model integration. However, as indicated in Fig. 5, the vortex moves with the lower-level flow. The vortex speed and direction are most closely approximated by the flow averaged over a circle of 300–400 km and 200 km, respectively, which is consistent with the findings of Wang and Li (1992).

b. Development of vertical tilt

The vortex tilts equatorward with height during the first 12 h of integration (Fig. 3b); the tilted axis then rotates cyclonically relative to the surface center (Fig. 3a). By 120 h, the vortex tilts poleward and westward, and the upper- and lower-level centers have rotated

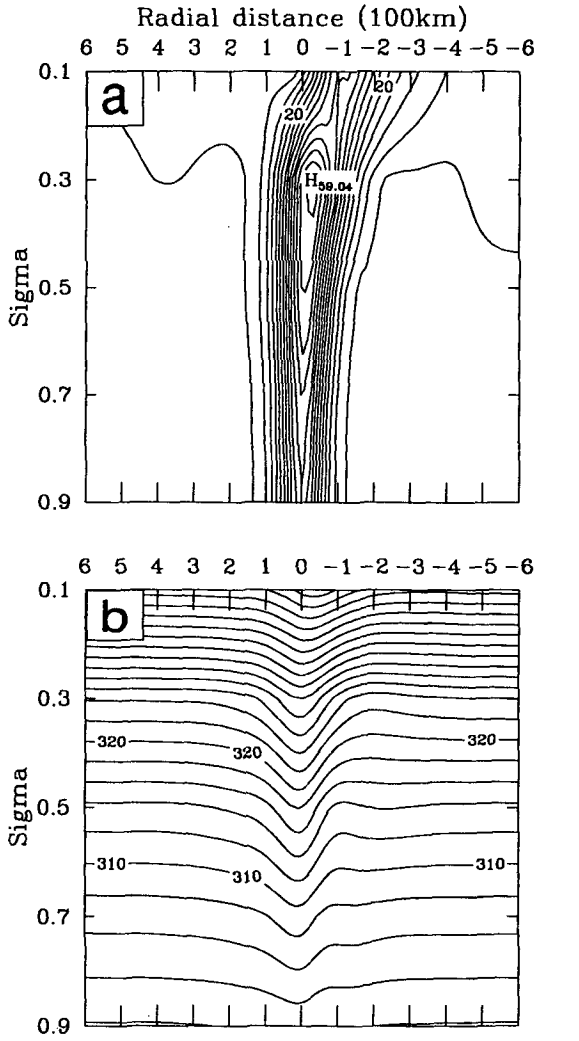

FIG. 6. Vertical cross sections at 96 h through the standard vortex centers at $\sigma = 0.1$ and $\sigma = 0.9$: (a) potential vorticity with contour interval of 4×10^{-7} K km^{-1} m^2 s^{-1} and (b) potential temperature with contour interval of 2.0 K.

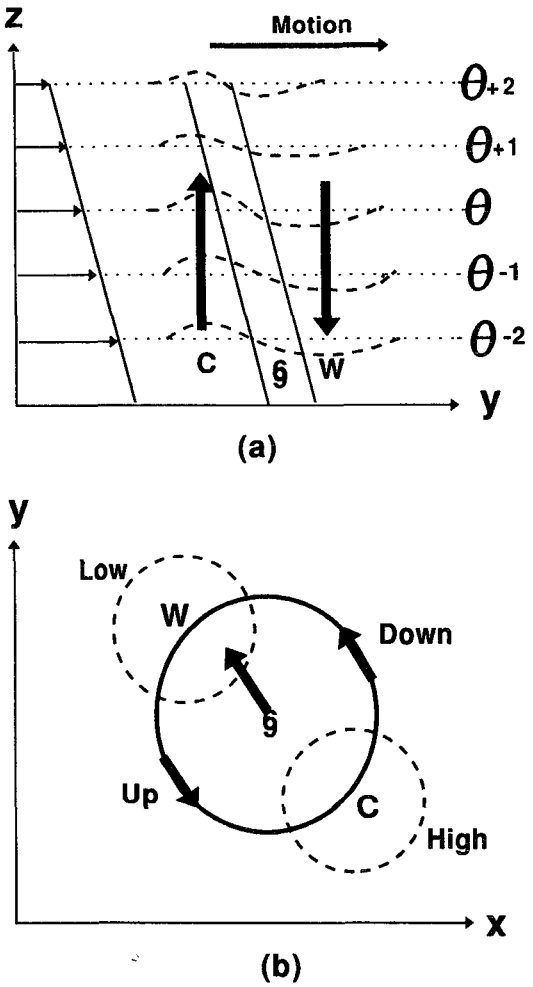

FIG. 7. Schematic of the mechanisms contributing to the development of a divergent circulation. (a) Arrows on the left of the panel indicate the northwestward ventilation flow over the vortex center caused by the beta effect, which decreases with height. The cyclone symbol indicates the surface vortex center, and the tilt of the vortex center is indicated. Dashed lines show the potential temperature anomalies required to balance the tilted vortex, which are achieved by vertical motion as indicated by the heavy arrows. (b) Plan view of the potential temperature anomalies. The regions within the dashed circles indicate the raised isentropes (High) where they are cooled (**C**) and the lowered isentropes (Low) where they are warmed (**W**). The bold circle indicates the relative motion of the cyclonic circulation of the main vortex through the potential temperature anomalies, which descends as it moves toward the region of lowered isentropes (Down) and ascends as it moves toward the region of raised isentropes (Up).

through 250°. We note that the vortex tilt is not uniform with height, being weak in the lowest four levels and marked between the upper two levels (Fig. 6). The upper shearing increases considerably with time, so that the centers are separated by about 200 km at 120 h.

Jones (1995) has shown that the initial effect of a baroclinic environmental flow is to tilt a cyclonic vortex downshear. The upper- and lower-level centers then start to rotate cyclonically about the midlevel center, as is observed in the present study (Fig. 3). The strength of the interaction depends on the penetration depth over which influence of the anomaly extends (Hoskins et al. 1985; Davis 1992), which can be expressed as a function of the scale and strength of the anomaly and the static stability of the environment. For a nearly axisymmetric vortex in hydrostatic and gradient balance, the penetration depth is (Hoskins et al. 1985; Shapiro and Montgomery 1993)

$$D = \frac{(f_{\text{loc}}\zeta_a)^{1/2}L}{N}, \tag{20}$$

where $f_{\text{loc}} = f + 2V_T/r$ and ζ_a is the vertical component of the absolute vorticity, L the length scale of the vor-

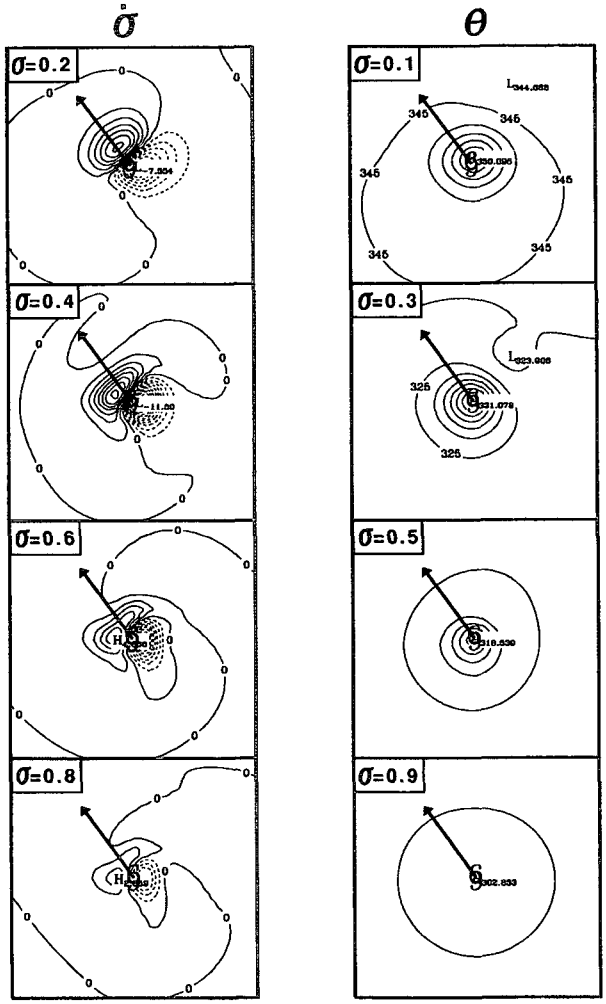

FIG. 8. Vertical σ velocity (left) and potential temperature (right) fields for the standard vortex after 60 h at the indicated σ levels. Contour intervals are 1×10^{-6} s^{-1} in the left panels and 1.0 K in the right panels. The domain shown in each panel is 800 km × 800 km. The cyclone symbol and arrow indicate the position and direction of motion of the vortex center at the lowest level.

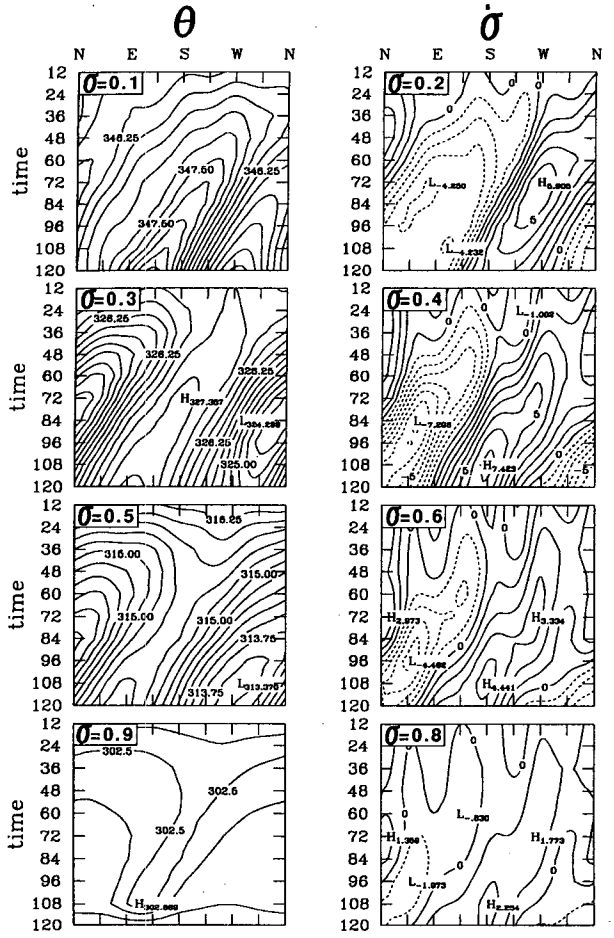

FIG. 9. Evolution of potential temperature (left panels) and vertical velocity at the indicated levels on a circle of 100-km radius from the standard vortex center, with compass direction indicated at the top and contour intervals of 0.25 K in left panels and 1×10^{-6} s^{-1} in the right panels.

tex, V_T the tangential wind of the vortex, and N the static stability. Equation (20) demonstrates that the vertical penetration depth of a PV anomaly is directly proportional to the strength, horizontal scale of the anomaly, and the local frequency of the rotation but inversely proportional to the static stability in its environment. For the standard vortex used here, the upper circulation is very weak, so that the influence of the upper-level anomaly on the lower-level motion is limited and consistent with the small cyclonic–anticyclonic curvature in the vortex track (Figs. 3a,b). However, the strong circulation at lower levels markedly influences the upper-level vortex motion (Fig. 3a). Note that the maximum PV anomaly at level 2 (Fig. 6a) is due to the maximum vertical gradient of potential temperature being located at that level (Fig. 6b). As a result, a smooth track is observed at this level, and the centers at all the other levels rotate about this center (Fig. 3a).

Interaction between circulations at different levels may reduce or enhance the vertical tilt of the vortex. For example, at 24 h the upper-level vortex centers are located to the east of the lowest-level center (Fig. 3a). Thus, a poleward flow across the upper-level vortex center from the projection of the associated lower-level PV anomaly tends to counteract the equatorward tilting effect of the beta gyres. At 120 h, the upper-level vortex centers are located to the west and poleward of the lowest-level center. Vertical projection of both the lower-level and upper-level PV anomalies acts to accelerate the cyclonic rotation of the tilted axis and to increase the beta-induced equatorward tilt of the vortex.

c. *The role of divergent circulation*

Wang and Li (1992) found that a baroclinic cyclone drifted poleward and westward with a nearly height-independent speed, which they suggested was related to the vertical mean relative angular momentum of the initial vortex. This behavior was attributed to the development of a divergent circulation, with vertical motion coupling the vortex cores. This finding is consistent with our standard vortex experiment (Fig. 3a), except that significant vertical tilt develops in the upper troposphere.

The questions arise as to how the divergent circulation develops and what role it plays in the beta drift of a baroclinic vortex. Jones (1995) used results obtained by Raymond (1992) to discuss the behavior of a tilted vortex in vertical shear on an f plane. She showed that the vertical circulation developed in a manner that is consistent with the model flow remaining balanced. We hypothesize here that such a consideration is also applicable to the tilted vortex due to the beta effect.

If the initial cyclonic PV anomaly is tilted in the vertical and the flow remains balanced, a potential temperature anomaly must develop in such a way that cooling (warming) occurs on the downtilt (uptilt) side of the vortex center. The only way of achieving the required thermal perturbation for adiabatic motion is through vertical advection (Jones 1995; Hoskins et al. 1985; Raymond 1992). Since the standard vortex initially tilted equatorward with height due to the differential beta effect (Fig. 3b), cooling and ascent (warming and descent) should develop on the equatorward (poleward) side of the vortex center, as illustrated in Fig. 7a. Once the thermal anomaly is adjusted to be in balance with the tilted PV anomaly, the isentropes become raised (lowered) in the downtilt (uptilt) direction. Cyclonic circulation across this anomaly produces a wavenumber one pattern of ascent and descent, with a phase shift of 90° from the thermal perturbation, as illustrated in Fig. 7b.

It is clear from the vertical motion fields after 60 h of integration (left panels in Fig. 8) that ascending mo-

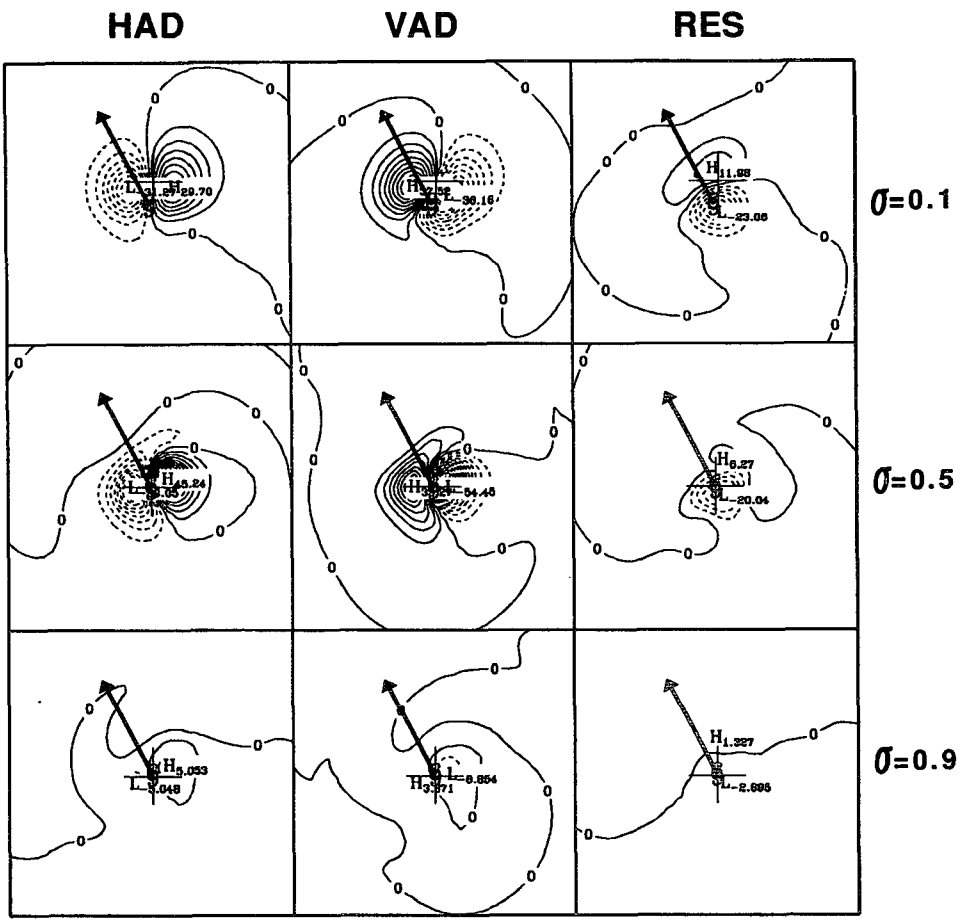

FIG. 10. Potential temperature budget for the standard vortex after 72 h at the indicated levels: left panels, horizontal advection (HAD); center panels, vertical advection (VAD); right panels, residual (RES). Contour interval is 4×10^{-5} K s^{-1}, and the domain shown in each panel is 800 km $\times$ 800 km. The cyclone symbol and arrow indicate the position and direction of motion of the vortex center at the lowest level, and the crosshairs indicate the positions of the vortex centers at the corresponding levels.

tion has developed to the southeast of the vortex center, with descending motion to the northwest, at a time when the vortex tilts northeastward (Fig. 3a). The vertical motion maxima have a phase shift of 90° relative to the potential temperature anomaly maxima (right panels in Fig. 8) and are located at the $\sigma = 0.4$ level and just within the radius of maximum wind, which is where the largest deformation of the isentropes develops (right panels in Fig. 8). These configurations are similar to those found by Jones (1995) and consistent with the schematic in Fig. 7b. Closer examination of other time periods (not shown) indicates that the relationship between the vertical motion and potential temperature anomalies is closely linked to the orientation of the vortex tilt. Thus, we concur with Jones in that the fundamental process is balance requirements on the tilted vortex, regardless of the cause of the tilt. It is not directly attributable to beta effects.

Figure 9 shows the time evolution of both the potential temperature (left panels) and vertical velocity (right panels) at the indicated levels on a circle of 100-km radius from the vortex center. The development and evolution of the potential temperature anomalies are consistent with the vertical tilt of the vortex, with cooling (warming) on the downtilt (uptilt) side (Figs. 3 and 9). However, a relatively complicated evolution of vertical motion is observed in Fig. 9. During the first 36 h, ascending (descending) motion is nearly stationary with the maximum on the equatorward (poleward) side of the vortex center. This vertical motion concurs with the development of the required thermal perturbation for the equatorward tilt of the vortex, as illustrated in Fig. 7a. The physical process illustrated in Fig. 7b also contributes to the evolution of vertical motion during this period.

Horizontal and vertical advection of potential temperature in our σ-coordinate system tend to cancel each other as the air flows along isentropes (Fig. 10). They should exactly cancel for a stationary vortex

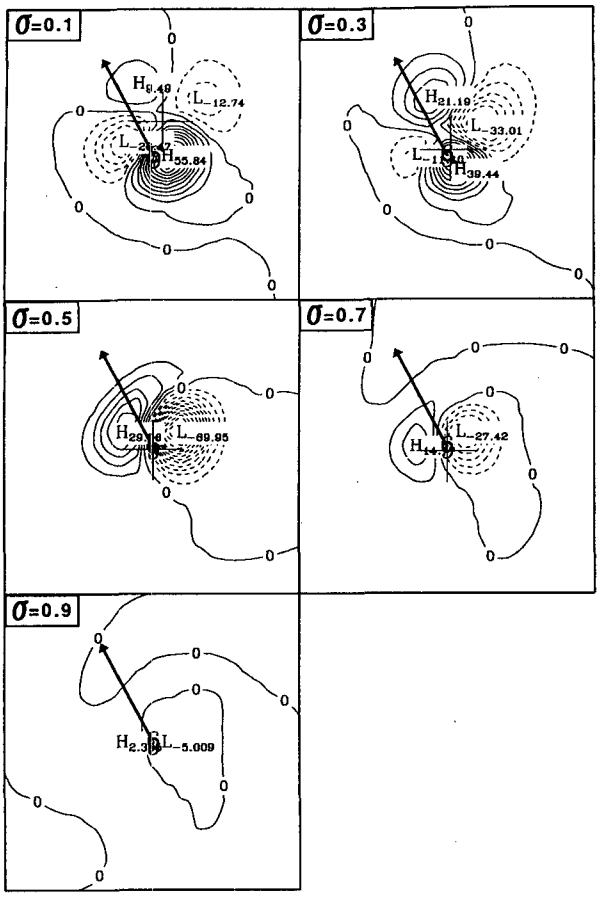

FIG. 11. Local change of potential vorticity by vertical advection at indicated levels after 72 h for the standard vortex. Contour interval is 0.5×10^{-12} K kg^{-1} m^2 s^{-2}, and the domain shown in each panel is 500 km × 500 km. The cyclone symbol and arrow indicate the position and direction of motion of the vortex center at the lowest level, and the crosshairs indicate the positions of the vortex centers at the corresponding levels.

(Hoskins et al. 1985). For the moving systems studied here, the residual of the horizontal and vertical advection corresponds to the potential temperature change required by motion of the vortex and the changing orientation of tilt with time, as indicated in Fig. 10.

Wang et al. (1993) and Holland and Wang (1995) found that the vertical divergent circulation may play an important role in maintaining a stable vortex tilt in a baroclinic environment. Such a mechanism seems not to be applicable to the standard vortex in this study. As illustrated in Fig. 11, vertical advection of potential vorticity after 72 h of integration merely slows down the cyclonic orbit of the upper- and lower-level vortex centers. It does not maintain the vortex in the vertical since the maxima of vertical advection of PV are nearly orthogonal to the direction of the tilted axis (Fig. 11).

4. Influence of vertical structure of the vortex

Wang and Li (1992) suggested that for cyclonic vortices the vertical structure affects the beta drift by changing the vertical MRAM, in a similar manner to that found for changes in horizontal structure by Shapiro and Ooyama (1990). However, when the vortex turns anticyclonic with height, the anticyclonic and cyclonic parts move essentially independently of each other, and substantial shearing occurs. This arises from the change of sign of the vertical motion associated with the processes described in the previous section, so that no vertical coupling holds the upper anticyclonic and lower cyclonic circulation together. We have shown that the vertical motion develops primarily to maintain the tilted vortex in a balanced state and not to keep the vortex vertical, as suggested by Wang and Li (1992). Further, Wu and Emanuel (1993) and Flatau et al. (1994) found that the cyclone motion was significantly influenced by displacement of the upper anticyclone. This produced movement of the whole vortex to the left of the vertical shear vector in the Northern Hemisphere.

The outer anticyclonic circulation in the upper troposphere is a common feature of tropical cyclones (Frank 1977), and we have constructed several vortices to simulate a variety of the tropical cyclonelike vortices labeled V_B, V_C, and V_D (see Table 1 and Fig. 1). Vortex V_B is similar to V_A, with a deep, strong cyclonic circulation overlayed by a very weak anticyclonic circulation at the uppermost level and large radius (Fig. 1b). Since the vertical MRAM in V_B is smaller than that in V_A (Fig. 2), the findings by Wang and Li (1992)

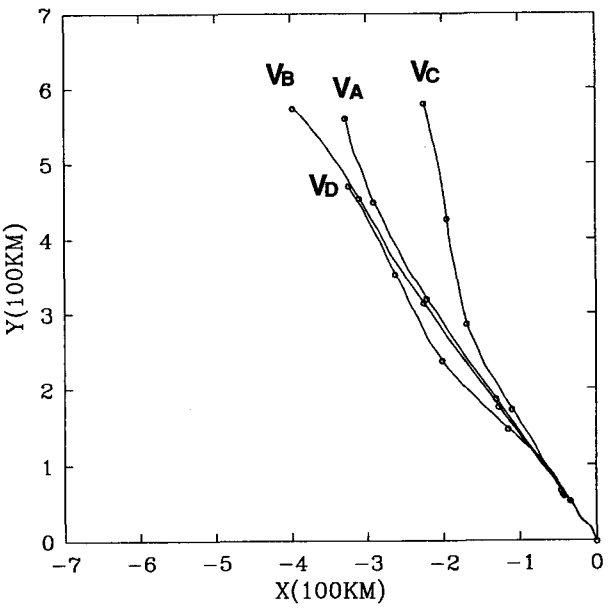

FIG. 12. 120-h tracks of the four vortices from Fig. 1, with 24-h positions indicated.

predict a slower beta-drift speed. But this is observed only for the motion during the first 48 h, after which V_B moves slightly faster and more westward than V_A (Fig. 12). This behavior suggests that vertical interactions between the tilted vortex circulations are more important in determining the motion.

During the first 48 h of integration, the upper-level anticyclone for V_B drifts equatorward and westward relative to the lower-level cyclonic vortex, so that vertical coupling slows the cyclone down (Fig. 13a). However, such an effect decreases toward the surface and helps the lower-level cyclonic portion of the vortex tilt farther eastward compared to vortex V_A (Figs. 13a and 14b). Upward projection of the lower-level PV anomaly advects the upper-level anticyclone eastward relative to the lower-level vortex (Fig. 13a). Since the anticyclonic PV anomaly is very weak, its vertical influence is very limited, and thus the lower tilted cyclone interaction dominates. The tilted axis rotated cyclonically through 360° between 36 and 120 h (Fig. 14b). After 72 h, the upper-level cyclonic PV anomaly in V_B is mainly located on the south or southeast side of the lowest-level center (Figs. 13b and 14b), leading to a slightly faster westward to northwestward motion than for V_A (Fig. 12). Upward motion arising from the tilted vortex advects cyclonic PV to create a new cyclonic core in the upper level (Fig. 15).

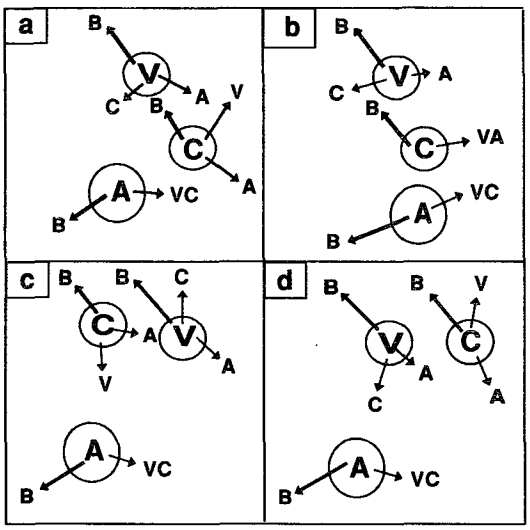

FIG. 13. Schematic of the interactions between the circulations at different vertical levels. The circled V, C, and A indicate the cyclonic PV anomaly at the surface, the cyclonic PV anomaly at the upper levels associated with the tilted vortex, and the anticyclonic PV anomaly at the top level, respectively. The big arrow with B denotes the motion component caused by the beta effect at the corresponding level; the thin arrows with V, C, and A indicate the motion components associated with the vertical projection of the corresponding PV anomalies. For example, the arrow with A in the circled V indicates the motion component of the surface vortex caused by the flow associated with the downward penetration of the upper-level anticyclonic PV anomaly.

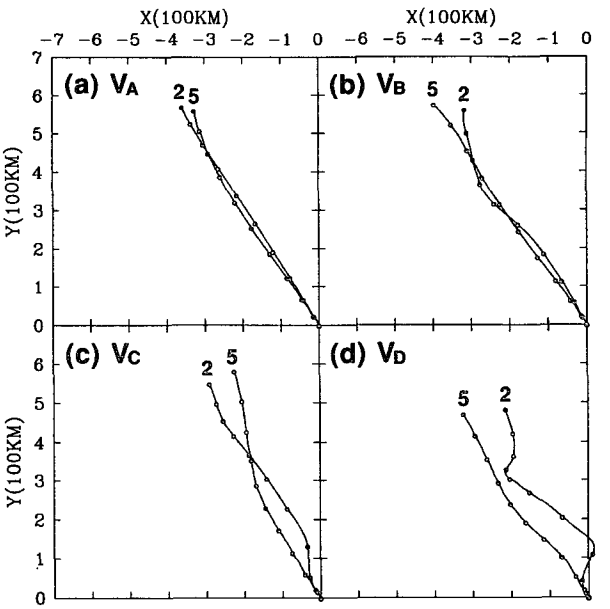

FIG. 14. 120-h trajectories of the four vortices at the second (2) and lowest (5) levels, indicating the development of vertical tilt of the vortices, with all 12-h positions shown.

The stronger anticyclone in V_C evolves to produce the sharp change of track near 60 h shown in Fig. 12. As the anticyclonic PV anomaly moves equatorward relative to the lower-level vortex core (Fig. 16), it introduces a poleward turning of the lower vortex and reduces the degree of cyclonic rotation of the tilted vortex axis (Fig. 14c). Flow associated with the downward penetration of the anticyclonic PV anomaly tilts the cyclonic portion of the vortex eastward. This, combined with interactions at lower levels, leads to a more eastward and poleward motion after 72 h of V_C compared to the other vortices (Figs. 12 and 13c). Similar mechanisms are applicable to V_D (Figs. 13d and 14d), which has the strongest and deepest upper-level anticyclone.

In summary, vertical interactions between the PV anomalies associated with a tilted vortex are important processes in baroclinic vortex motion. Such interactions become more complicated for a vortex with an upper anticyclone, such as occurs for tropical cyclones, than for a uniformly cyclonic vortex. Then a complex vertical coupling between anticyclonic and cyclonic PV anomalies can substantially influence the vortex motion.

5. Sensitivity experiments

The results obtained in the last two sections have shown that the beta drift of a baroclinic vortex is determined both by the flow related to the beta gyres and flow associated with the vertical projection of the tilted PV anomalies. The strength of this second vertical in-

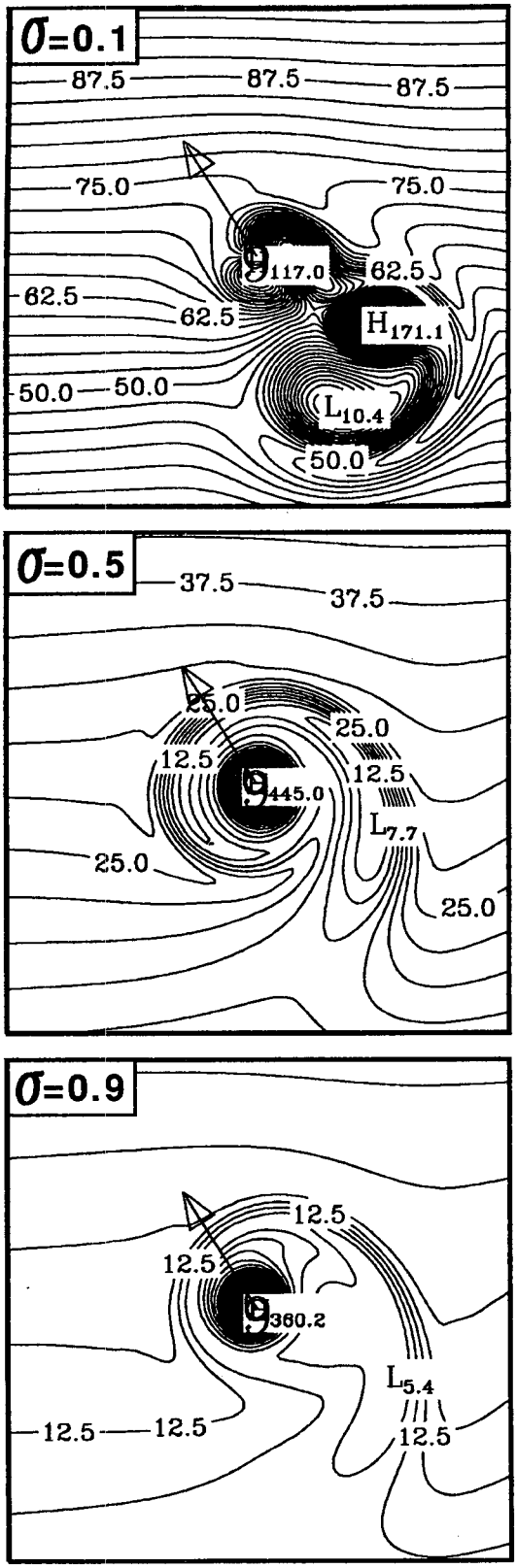

FIG. 15. Potential vorticity fields at indicated levels for V_B after 96 h. Contour interval is 2.5×10^{-8} K kg^{-1} m^2 s^{-1}.

teraction depends on the penetration depth of the anomaly, which is a function of the Coriolis parameter, static stability, and the horizontal scale and strength of the vortex [Eq. (20)]. In this section several experiments are conducted to examine the sensitivity of the beta drift to these parameters.

a. Sensitivity to initial latitude

Wang and Li (1992) found a significant latitudinal dependence of the beta drift, which decreased by about 45% when the starting latitude was varied from 10°–30°N. They noted that this latitudinal dependence could not be completely explained by the 11% change of earth vorticity gradient, but it could be associated with the threefold increase of the Coriolis parameter. Our experiments over 120-h periods for vortices starting at 10° and 20°N (Fig. 17) indicate that the monotonic changes indicated by Wang and Li do not hold. Significant track deviations occur after 72 h, and, especially for V_C, the net drift "increases" with latitude. These track deviations are consistent with an increased vertical coupling associated with the evolving vertical structure discussed in previous sections. For example, the rotation rates of the upper and lower centers are weaker for the 10°N vortices, which concurs with a shallower vertical penetration depth [Eq. (20)]. We therefore conclude that part of the latitudinal variation in vortex motion arises from the changing degree of vertical projection of PV anomalies.

b. Sensitivity to static stability

Sensitivity to the degree of static stability was tested by conducting experiments with double the static stability (S2 in Fig. 18) to that used in the standard run. This gives similar results to the change in Coriolis parameter, as expected from the reduction of penetration depth [Eq. (20)]. Our results are consistent with the findings of Jones (1995). Wang and Li (1992) found that the beta drift is almost independent of static stability, which is surprising given the requirement for a strong vertical motion to maintain the vertical structure of their vortex. We suggest that this finding is due to the short time integration of 48 h used by Wang and Li, which is insufficient for development of significant vertical tilt. The influence of development of vertical tilt is clearly indicated by the sharp changes in tracks in Fig. 18.

c. Sensitivity to horizontal scale of the vortex

Changing the radius of the maximum wind in Eq. (15) changes the horizontal scale of the cyclonic component of the vortices and thus both the penetration depth [Eq. (20)] and the beta drift (e.g., Chan and Williams 1987; Fiorino and Elsberry 1989a,b; Wang and Li 1992). Our experiments clearly indicate (Fig.

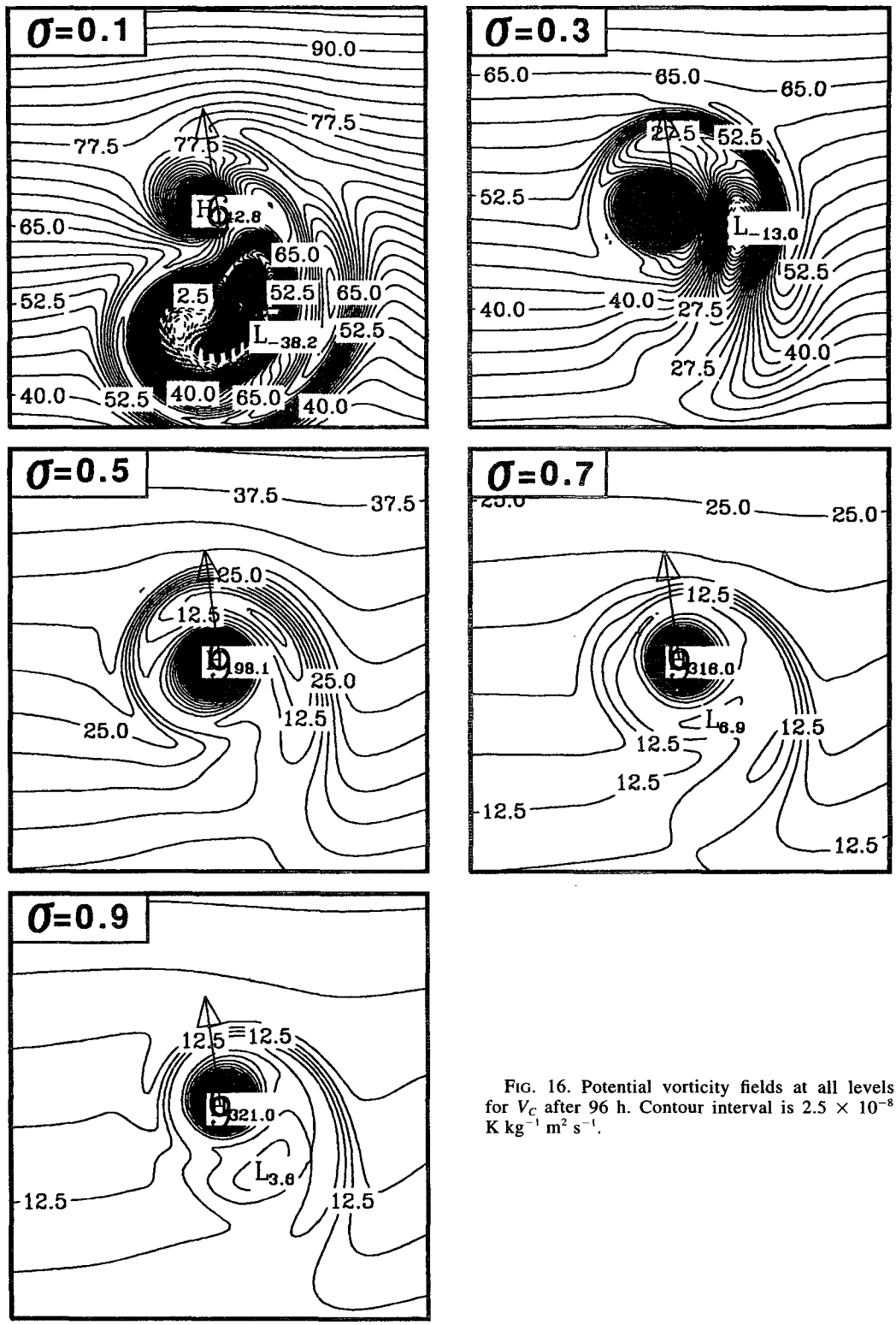

FIG. 16. Potential vorticity fields at all levels for V_C after 96 h. Contour interval is 2.5×10^{-8} K kg^{-1} m^2 s^{-1}.

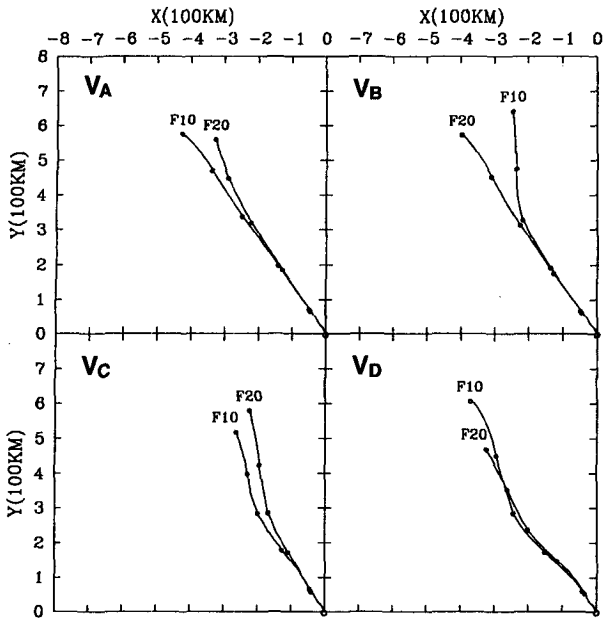

FIG. 17. 120-h tracks of the four vortices from Fig. 1, with 24-h positions indicated. F10 and F20 indicate the initial latitude of the vortices at 10° and 20°N, respectively.

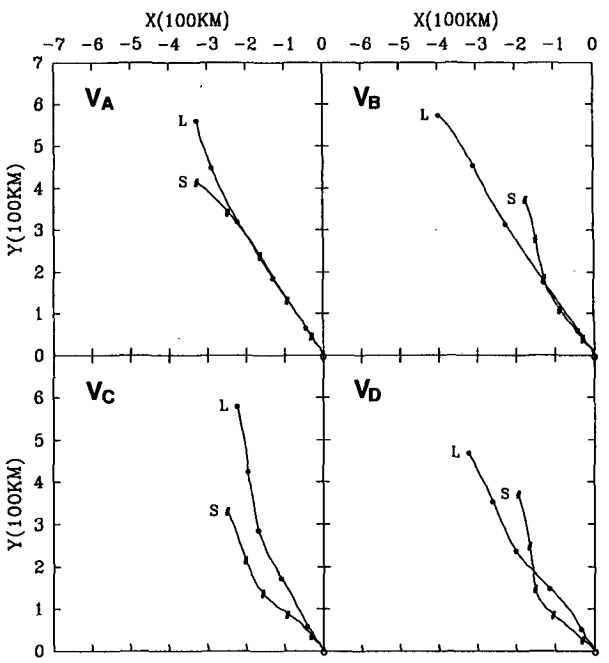

FIG. 19. 120-h tracks of the four vortices from Fig. 1, with 24-h positions indicated, comparing standard (L) and small (S) vortices.

19) that reducing the vortex size (by reducing r_m to 75 km) causes slower movement than that which can be explained by the scale dependence of the beta drift alone.

We suggest that both the vertical structure and degree of vertical coupling contribute to the changed motion and illustrate this with three examples. The rotation rate of the tilted axis is slower for small vortices. Sec-

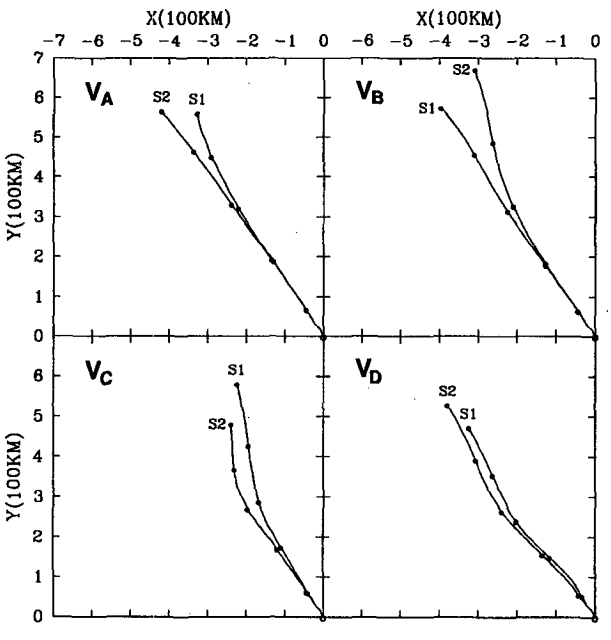

FIG. 18. 120-h tracks of the four vortices from Fig. 1, with 24-h positions indicated, comparing standard (S1) and doubled (S2) static stability.

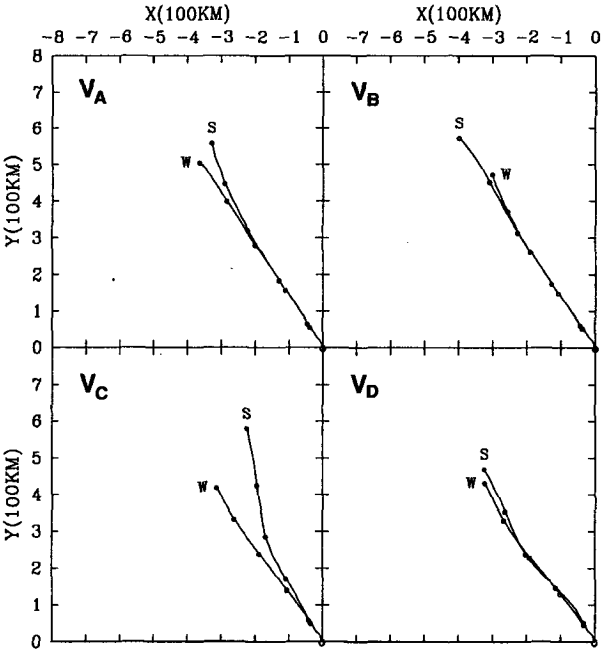

FIG. 20. 120-h tracks of the four vortices from Fig. 1, with 24-h positions indicated, comparing standard (S) and weak (W) vortices.

ond, for the completely cyclonic vortex V_A the small vortex tilts northeast during the last 24 h, and vertical coupling deflects the surface center to the left of the larger vortex track (Fig. 19). Third, for vortex V_B, the upper-level anticyclonic circulation is kept identical for both small and large cyclones. Thus, when the anticyclone moves toward the southwest, the flow projected onto the lower levels advects the cyclone to the east and causes a more northeastward tilt. This further reduces both the meridional and zonal components of the beta drift.

d. Sensitivity to the strength of the initial vortex

The response to a 30% reduction of the strength of circulation in both the cyclonic and anticyclonic components of the initial vortices is illustrated in Fig. 20. Smith (1993) suggested that the beta-drift speed of a barotropic vortex is proportional to the square root of the maximum wind. Wang and Li (1992) found a dependence of beta drift on the vertical mean relative angular momentum of a baroclinic vortex. These results are qualitatively reproduced for the first 72 h of all experiments, but they are significantly modified by vertical coupling once vortex tilt develops. The processes follow those described in the previous sections. Reducing the vortex strength is equivalent to reducing the vertical penetration depth [Eq. 20] and, thus, the degree of vertical interaction. Since the four weaker vortices have the same cyclonic circulation at the lowest two levels, it is expected that they should have similar tracks, which is evident in Fig. 20.

6. Comparison with the equivalent barotropic motion

The motion of the four benchmark baroclinic vortices studied in sections 3 and 4 is compared with that of the corresponding equivalent barotropic vortices. For the cyclonic vortex V_A, the baroclinic vortex track (BC in Fig. 21a) is similar to that for the equivalent barotropic vortex (BT in Fig. 21a). Vertical coupling mechanisms cause the baroclinic vortex to move slightly faster than, and to the right of, the equivalent barotropic system after 72 h. This result suggests that barotropic mechanisms may dominate the motion of uniformly cyclonic, adiabatic baroclinic vortices.

The baroclinic motion of the three tropical cyclone–like vortices, however, is very different from the corresponding equivalent barotropic motion (Figs. 21b,c,d). The barotropic motion is nearly proportional to the MRAM (comparing Fig. 21 with Fig. 2) of the initial vortex, as found in previous studies (e.g., Shapiro and Ooyama 1990). Our experiments (Fig. 21) indicate that the baroclinic vortices move consistently faster and more westward than the corresponding equivalent barotropic systems.

An important aspect should be mentioned here. In the equivalent barotropic model, the original upper-level anticyclonic circulation is directly projected onto the integral vortex. It thus directly affects the radial structure of the cyclone, which moves more poleward and slower as the upper anticyclone intensifies (e.g., V_D in Fig. 21). However, in the baroclinic vortex the influence of the upper-level anticyclone on the motion of the surface vortex depends on the vertical penetration depth and the degree of shearing that occurs. As a marked vortex tilt develops, vertical interaction has a significant, nonlinear impact on the vortex motion.

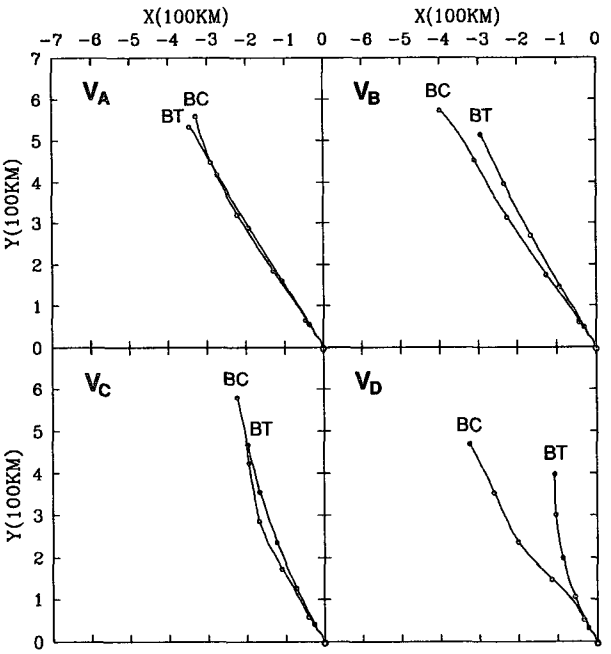

FIG. 21. 120-h tracks of V_A, V_B, V_C, and V_D on the beta plane from the baroclinic model (BC), and the corresponding tracks of the equivalent barotropic vortices from a barotropic model (BT); 24-h positions are indicated.

7. Conclusions

The movement of an initially axisymmetric baroclinic vortex embedded in an environment at rest on a beta plane has been investigated with a three-dimensional primitive equation model. Attention was given to the motion and evolution of an adiabatic vortex and the influence of the vertical structure of the vortex and vertical coupling mechanisms.

All vortices moved poleward and westward following interaction with the earth vorticity gradient, as has been extensively studied for barotropic vortices (Fiorino and Elsberry 1989a,b; Chan and Williams 1987) and extended to baroclinic vortices by Wang and Li (1992). However, we find that vertical tilt produces significant changes to the basic motion as different levels interact following the general mechanisms described by Hoskins et al. (1985) and applied to tropical

cyclones by Wu and Emanuel (1993), Flatau et al. (1994), and Jones (1995). While we concur with the general findings of these latter studies, we find the motion in an earth vorticity gradient to be more complex than that found by Wu and Emanuel (1993) in their two-level quasigeostrophic model and that discussed by Jones (1995) for an initially barotropic vortex in vertical shear.

Initially, a purely cyclonic vortex tilts equatorward due to the differential beta-effect propagation, which decreases with height. The tilted axis then rotates cyclonically relative to the surface vortex center due to coupling between the tilted potential vorticity anomalies. A balance develops in which both the advecting flow associated with the beta effect and the vertical projection of the tilted PV anomaly act to move the vortex.

A divergent circulation develops from the following process: if a cyclonic potential vorticity anomaly is tilted in the vertical, dynamical balance requires development of a potential temperature anomaly with cooling on the downtilt side and warming on the uptilt side of the vortex center. This is achieved by adiabatic vertical motion (Fig. 7a). Provided that the flow remains balanced, the air parcels moving along isentropic surfaces will ascend when moving toward the cool anomaly and descend toward the warm anomaly. A wavenumber one pattern of ascent and descent therefore develops, with a phase shift of 90° from the potential temperature anomaly (Fig. 7b). In contrast to the suggestions by Wang and Li (1992), we find that the vertical circulation is a direct consequence of balance requirements in the tilted vortex. It tends to slow down the cyclonic rotation of the upper and lower vortex centers.

Both the development of the vortex tilt and the corresponding divergent circulation strongly depend on its vertical structure, size, and intensity, as well as external parameters, such as the earth rotation and static stability of the environment. These parameters influence the motion of the vortex by changing the amplitude and the orientation of beta gyres and/or changing the penetration depth of a PV anomaly.

For tropical cyclone–like vortices, the shearing of the upper anticyclonic circulation can have a significant impact on the translation of the surface vortex. This is consistent with, but much more complicated than, the findings of Wu and Emanuel (1993) and Flatau et al. (1994) and differs from the small effect found by Wang and Li (1992).

We find that uniformly cyclonic vortices move nearly with equivalent barotropic motion. However, the motion is very different when the vortex turns anticyclonic with height, which results from the evolving influence of vortex tilt. Because of this influence, we find that the dependence on mean relative angular momentum (MRAM) suggested by Wang and Li (1992) applies only to the first 48–72 h of integration. Longer integrations do not display a consistent relationship between motion and MRAM.

These results are for adiabatic systems. Diabatic heating introduces an additional divergent circulation that could directly influence the vertical structure and tilt and thus the vortex motion. However, we shall show in Part II of this study that the basic mechanisms discussed here still play an important role in the motion of baroclinic vortices with cumulus convection. For example, the adiabatic vertical circulation associated with the vertically tilted vortex may contribute to the development of asymmetries in cumulus convection within the vortex circulation and thus further influence the vortex motion.

Acknowledgments. Many thanks are due to Dr. Lance Leslie for his help with the numerical model and to Liz Ritchie for carefully reading an early version of the manuscript. Part of this work has been sponsored by the U.S. Office of Naval Research under Contract N-00014-94-1-0556.

REFERENCES

Arakawa, A., and V. R. Lamb, 1977: Computational design of the basic dynamical process of the UCLA general circulation model. *Methods in Computational Physics,* Vol. 17, Academic Press, 173–265.

Carr, L. E., 1989: Barotropic vortex adjustment to asymmetric forcing with application to tropical cyclones. Ph.D. dissertation, Naval Postgraduate School, Monterey, CA, 143 pp.

——, and R. T. Williams, 1989: Barotropic vortex stability to perturbations from axisymmetry. *J. Atmos. Sci.,* **46,** 3177–3196.

Chan, J. C.-L., and R. T. Williams, 1987: Analytical and numerical studies of the beta-effect in tropical cyclone motion. Part I: Zero mean flow. *J. Atmos. Sci.,* **44,** 1257–1265.

Davis, C. A., 1992: Piecewise potential vorticity inversion. *J. Atmos. Sci.,* **49,** 1397–1411.

DeMaria, M., 1985: Tropical cyclone motion in a nondivergent barotropic model. *Mon. Wea. Rev.,* **113,** 1199–1210.

Elsberry, R. L., and R. F. Abbey Jr., 1991: Recent advances in the understanding of tropical cyclone motion. Tech. Rep. NPS-MR-91-003, Naval Postgraduate School, 92 pp. [Available from Naval Postgraduate School, Monterey, CA 93943.]

Fiorino, M., and R. L. Elsberry, 1989a: Some aspects of vortex structure related to tropical cyclone motion. *J. Atmos. Sci.,* **46,** 975–990.

——, and ——, 1989b: Contributions to tropical cyclone motion by small, medium, and large scales in the initial vortex. *Mon. Wea. Rev.,* **117,** 721–727.

Flatau, M., and D. E. Stevens, 1989: Barotropic and inertial instabilities in a hurricane outflow layer. *Geophys. Astrophys. Fluid Dyn.,* **47,** 1–18.

——, and ——, 1993: The role of outflow-layer instabilities in tropical cyclone motion. *J. Atmos. Sci.,* **50,** 1721–1733.

——, W. H. Schubert, and D. E. Stevens, 1994: The role of baroclinic processes in tropical cyclone motion: The influence of vertical tilt. *J. Atmos. Sci.,* **51,** 2589–2601.

Frank, W. M., 1977: The structure and energetics of the tropical cyclones I. Storm structure. *Mon. Wea. Rev.,* **105,** 1136–1150.

Gadd, A. J., 1978: A split explicit integration scheme for numerical weather prediction. *Quart. J. Roy. Meteor. Soc.*, **104,** 569–582.

——, 1980: Two refinements of the split explicit integration scheme. *Quart. J. Roy. Meteor. Soc.*, **106,** 215–220.

Holland, G. J., 1983: Tropical cyclone motion: Environmental interaction plus a beta effect. *J. Atmos. Sci.*, **40,** 68–75.

——, and Y. Wang, 1995: Baroclinic dynamics of simulated tropical cyclone recurvature. *J. Atmos. Sci.*, **52,** 410–426.

Hoskins, B. J., M. E. McIntyre, and A. W. Robertson, 1985: On the use and significance of isentropic potential vorticity maps. *Quart. J. Roy. Meteor. Soc.*, **111,** 877–946.

Jones, S. C., 1995: The evolution of vortices in vertical shear. Part I: Initially barotropic vortices. *Quart. J. Roy. Meteor. Soc.*, **121,** 821–851.

Leslie, L. M., and R. J. Purser, 1991: High-order numerics in an unstaggered three-dimensional time-split semiLagrangian forecast model. *Mon. Wea. Rev.*, **119,** 1612–1623.

Li, X., and B. Wang, 1994: Barotropic dynamics of the beta gyres and beta drift. *J. Atmos. Sci.*, **51,** 746–756.

McGregor, J. L., 1986: Accuracy and initialisation of a two-level split semi-Lagrangian scheme. *Short and Medium-Range Numerical Weather Prediction,* T. Matsuno, Ed., Meteor. Soc. Japan, 233–246.

Mesinger, F., 1977: Forward–backward scheme and its use in a limited-area model. *Contrib. Atmos. Phys.*, **50,** 200–210.

Peng, M. S., and R. T. Williams, 1990: Dynamics of vortex asymmetries and their influence on vortex motion on a β-plane. *J. Atmos. Sci.*, **47,** 1987–2003.

Purser, R. J., and L. M. Leslie, 1988: A semi-implicit, semi-Lagrangian finite-difference scheme using high-order spatial differencing on a nonstaggered grid. *Mon. Wea. Rev.*, **116,** 2069–2080.

Raymond, D. J., 1992: Nonlinear balance and potential-vorticity thinking at large Rossby number. *Quart. J. Roy. Meteor. Soc.*, **118,** 987–1015.

Shapiro, L. J., 1992: Hurricane vortex motion and evolution in a three-layer model. *J. Atmos. Sci.*, **49,** 140–153.

——, and V. Ooyama, 1990: Barotropic vortex evolution on a beta plane. *J. Atmos. Sci.*, **47,** 170–187.

——, and M. T. Montgomery, 1993: A three-dimensional balance theory for rapidly rotating vortices. *J. Atmos. Sci.*, **50,** 3322–3335.

Smith, R. B., 1993: A hurricane beta-drift law. *J. Atmos. Sci.*, **50,** 3213–3215.

Smith, R. K., and W. Ulrich, 1990: An analytical theory of tropical cyclone motion using a barotropic model. *J. Atmos. Sci.*, **47,** 1973–1986.

——, ——, and G. Dietachmayer, 1990: A numerical study of tropical cyclone motion using a barotropic model. Part I: The role of vortex asymmetries. *Quart. J. Roy. Meteor. Soc.*, **116,** 337–362.

Stevens, D. E., R. S. Lindzen, and L. J. Shapiro, 1977: A new model of tropical waves incorporating momentum mixing by cumulus convection. *Dyn. Atmos. Oceans,* **1,** 365–425.

Sutyrin, G. G., and G. R. Flierl, 1994: Intense vortex motion on the beta plane: Development of the beta gyres. *J. Atmos. Sci.*, **51,** 773–790.

Wang, B., and X. Li, 1992: The beta drift of three-dimensional vortices: A numerical study. *Mon. Wea. Rev.*, **120,** 579–593.

Wang, Y., 1995: On an inverse balance equation in sigma coordinates for model initialization. *Mon. Wea. Rev.*, **123,** 482–488.

——, and Y. Zhu, 1989: A numerical study on the Fujiwhara effect of two interacting cyclonic vortices (in Chinese). *J. Acad. Meteor. Sci., SMA,* **4,** 13–19.

——, G. J. Holland, and L. M. Leslie, 1993: Some baroclinic aspects of tropical cyclone motion. *Tropical Cyclone Disasters,* J. Lighthill, K. Emanuel, and G. J. Holland, Eds., Peking University Press, 280–285.

Willoughby, H. E., 1992: Linear motion of a shallow-water barotropic vortex as an initial-value problem. *J. Atmos. Sci.*, **49,** 2015–2031.

——, 1994: Nonlinear motion of a shallow water barotropic vortex. *J. Atmos. Sci.*, **51,** 3722–3744.

Wu, C.-C., and K. A. Emanuel, 1993: Interaction of a baroclinic vortex with background shear: Application to hurricane movement. *J. Atmos. Sci.*, **50,** 62–76.